Facilitating RNA Structure Prediction with Microarrays†

Elzbieta Kierzek,‡,§ Ryszard Kierzek,‡ Douglas H. Turner,*,§,|| and Irina E. Catrina§,⊥

Department of Chemistry, University of Rochester, RC Box 270216, Rochester, New York 14627-0216, Department of Pediatrics and Center for Pediatric Biomedical Research, School of Medicine and Dentistry, University of Rochester, Rochester, New York 14642, and Institute of Bioorganic Chemistry, Polish Academy of Sciences, Noskowskiego 12/14, 61-704 Poznan, Poland

Received July 19, 2005; Revised Manuscript Received October 21, 2005

ABSTRACT: Determining RNA secondary structure is important for understanding structure−function relationships and identifying potential drug targets. This paper reports the use of microarrays with heptamer 2′-*O*-methyl oligoribonucleotides to probe the secondary structure of an RNA and thereby improve the prediction of that secondary structure. When experimental constraints from hybridization results are added to a free-energy minimization algorithm, the prediction of the secondary structure of *Escherichia coli* 5S rRNA improves from 27 to 92% of the known canonical base pairs. Optimization of buffer conditions for hybridization and application of 2′-*O*-methyl-2-thiouridine to enhance binding and improve discrimination between AU and GU pairs are also described. The results suggest that probing RNA with oligonucleotide microarrays can facilitate determination of secondary structure.

The rapid increase in the size of the genome sequence database is making computational analysis of RNA increasingly important for revealing structure−function relationships and potential drug targets. While NMR and X-ray crystallography can definitively determine RNA structure, they cannot keep pace with the rapid generation of genomic data. Thus, faster methods are required to allow accurate modeling of RNA structures. The first step in this modeling is the prediction of secondary structure.

Prediction of RNA secondary structure is done mainly by two methods. One is sequence comparison (*1*−*5*). This method is based on finding structural features conserved during evolution. Most of the currently accepted RNA secondary structures were generated by this method, which is limited by sequence diversity and structural similarity within an RNA family. The second method uses thermodynamics to predict secondary structure by free-energy minimization. For example, computer programs, such as MFOLD and RNAstructure (*6*, *7*), use a nearest neighbor energetic model (*7*−*11*) to generate a lowest free-energy RNA secondary structure, as well as suboptimal structures with higher free energies. When tested against a database of about 150 000 nucleotides of known structures, the predicted lowest free-energy structure on average contains 73% of the known canonical base pairs (*7*). There are many RNA structures that are poorly predicted, however. Algorithms can include nuclease (*6*, *12*) or chemical mapping (*13*) data to constrain certain nucleotides and thereby improve predictions. Presumably, additional data from other types of experiments can further improve predictions. Here, we demonstrate that oligonucleotide microarrays allow rapid probing of RNA secondary structure and thus comparisons that can improve RNA structure prediction by computational methods.

Doty, Uhlenbeck, and Lewis (*14*−*16*) described an equilibrium dialysis binding assay that revealed single-stranded nucleotides in tRNA and 5S rRNA by binding of trimer and tetramer oligonucleotides. Although these dialysis experiments yield valuable information, they are slow. A faster way to obtain similar data is to use microarrays of oligonucleotides, which allow many more oligonucleotides to be screened in parallel for binding to an RNA. For example, Southern and co-workers used microarrays to develop antisense candidates for mRNA (*17*−*19*). Activated glass slides are used for clever *in situ* synthesis of oligonucleotides that vary in length from 1 to 20 nucleotides and are complementary to the RNA of interest. Thus, a microarray is custom-prepared for a given mRNA.

If oligonucleotide length is restricted, then it becomes feasible to make a microarray with all possible sequences of a given length. For example, Mirzabekov and co-workers studied the stability and specificity of all hexamers immobilized on a chip made with activated polyacrylamide gel pads (*20*). Relative to arrays coated on a 2D surface, gel-coated slides provide an advantage for detection because the 3D matrix allows more probe to be loaded.

Here, we show that immobilized heptamers can hybridize to *Escherichia coli* 5S rRNA and can be used to probe its secondary structure. The native secondary structure, form A, of *E. coli* 5S rRNA is known from sequence alignments (*1*, *21*) and has been confirmed by NMR of fragments (*22*), by X-ray crystallography of a fragment (*23*), and by comparison to the X-ray structure of the large ribosomal subunit of *Haloarcula marismortui* (*24*). Current versions

† This work was supported by NIH Grants GM2939 (to D.H.T.) and 1R03 TW1068 (to R.K. and D.H.T.).

* To whom correspondence should be addressed. Telephone: (585) 275-3207. Fax: (585) 276-0205. E-mail: turner@chem.rochester.edu.

‡ Polish Academy of Sciences.

§ Department of Chemistry, University of Rochester.

|| Department of Pediatrics and Center for Pediatric Biomedical Research, School of Medicine and Dentistry, University of Rochester.

⊥ Present address: University of Massachusetts Medical School, Program in Molecular Medicine and CFAR, Worcester, MA 01605.

10.1021/bi051409+ CCC: $33.50
Published on Web 12/17/2005

of the computer programs MFOLD (*7*) and RNAstructure (*13*), however, only predict 27% of the canonical base pairs in the accepted structure. We show that comparisons with experimental data generated with an oligonucleotide array can improve this prediction. Under non-native conditions, *E. coli* 5S rRNA folds into a different secondary structure, denoted as form B (*25*−*28*). Form B binds to microarrays very differently from form A.

MATERIALS AND METHODS

Materials. Standard phosphoramidites for oligonucleotide synthesis and C6 aminolinker were purchased from Glen Research. The [γ-^{32}P]ATP, T4 polynucleotide kinase, and T4 RNA ligase were purchased from Perkin−Elmer, Invitrogen, and Fermentas, respectively. RNases V1 and T1 were from Ambion, and nuclease S1 was from Fermentas. Dimethyl sulfate (DMS)[1] and 1-cyclohexyl-3-(2-morpholinoethyl)carbodiimide metho-*p*-toluenesulfonate (CMCT) were from Aldrich, and kethoxal was from ICN Biomedicals, Inc. *N*-methylisatoic anhydride (NMIA) was from Molecular Probes. Reverse transcriptase SuperScript III was from Invitrogen, and dNTPs and ddNTPs were from Amersham Biosciences. Agarose was a product of Invitrogen. Silanized slides and probe-clip press seal incubation chambers for hybridization experiments were purchased from Sigma. RNAsin and ribonuclease H were from Promega.

Chemical Synthesis of Oligonucleotides. Oligonucleotides were synthesized by the phosphoramidite approach on an ABI 392 synthesizer (*29*, *30*). The 2′-*O*-methyl-oligoribonucleotides used as probes for microarrays were synthesized with a C6 aminolinker on the 5′ end. Oligonucleotides were deprotected and purified according to published procedures (*9*), and molecular weights were confirmed by mass spectrometry (LC MS Hewlett−Packard series 1100 MSD with API-ES). Concentrations of all oligonucleotides were determined from predicted extinction coefficients for RNA (*31*) and measured absorbance at 260 nm at 80 °C.

Isolation of 5S rRNA. The *E. coli* 5S rRNA was prepared from *E. coli* carrying the overproducing plasmid pKK5-1 as previously reported (*32*), with some modification. Total RNA was fractionated by electrophoresis on an 8% polyacrylamide denaturing gel. The band corresponding to 5S rRNA was cut out and extracted with water by a crush and soak procedure with stirring at 4 °C overnight. The aqueous solution was concentrated with an equal volume of 2-butanol, and the RNA was precipitated with ethanol [2.5:1 ethanol/water (v/v)]. After centrifugation, the pellet was dissolved in water and the 5S rRNA concentration was determined by measuring the absorbance at 260 nm at room temperature using an extinction coefficient of 1.2×10^6 M^{-1} cm^{-1}. The sequence of the 5S rRNA was confirmed by reverse transcription dideoxy sequencing in a manner similar to that described by Merino et al. (*33*).

Folding of 5S rRNA. The 5S rRNA was annealed by heating for 5 min at 65 °C and then slowly cooled (0.5 °C/min) to room temperature (*25*). For most experiments, one of the following buffers was used for folding: (A) buffer 1Na$^+$/4Mg^{2+}/10T (1 M NaCl, 4 mM $MgCl_2$, and 10 mM Tris-HCl at pH 7.43), (B) buffer 0.15Na$^+$/4Mg^{2+}/10T (150 mM NaCl, 4 mM $MgCl_2$, and 10 mM Tris-HCl at pH 7.43), or (C) buffer 0.04Na$^+$/10Mg^{2+}/10T (40 mM NaCl, 10 mM $MgCl_2$, and 10 mM Tris-HCl at pH 7.43). For some experiments, the 5S rRNA was folded into form B according to a published procedure (*25*): 5S rRNA was incubated in 20 mM sodium borate, 7 M urea, and 250 mM Tris-HCl at pH 7.8 and 25 °C for 45 min, then quickly chilled at −15 °C for 3 min, and precipitated with 2.5 volumes of ethanol. The 5S rRNA precipitate was diluted in buffer 1Na$^+$/250T (1 M NaCl and 250 mM Tris-HCl at pH 7.8) at 0 °C.

Native Gel Electrophoresis. Native gel electrophoresis was done at 4 °C on a 10% polyacrylamide nondenaturing gel containing 40 mM Tris-acetate at pH 8.3, with a running buffer of 40 mM Tris-acetate at pH 8.3. The gel was preelectrophoresed at 150 V for 2 h. Electrophoresis was at 100−200 V for 48 h.

Enzymatic Mapping. RNase V1, RNase T1, and nuclease S1 were used for enzymatic mapping. The 5S rRNA was ^{32}P-radiolabeled at the 5′ or 3′ end. For enzymatic digestion, 2 pmol of 5S rRNA was used for each reaction and tRNA carrier was added to give a total RNA concentration of 8 μM. The following concentrations of enzymes were used for cleavage reactions: RNase V1 (0.005 unit/μL), RNase T1 (0.02 unit/μL), and nuclease S1 (2.5 units/μL). After annealing of 5S rRNA in buffer 1Na$^+$/4Mg^{2+}/10T, adding $ZnCl_2$ to a final concentration of 1 mM for the S1 reaction, and adding the appropriate enzyme, the solution was incubated at room temperature for 30 min. Reactions were stopped by ethanol precipitation on dry ice. After centrifugation, the pellet was dissolved in loading buffer and the reaction mixtures were analyzed on a 12% polyacrylamide denaturing gel. Cleavage products were analyzed by a comparison to ladders obtained from formamide treatment and from partial T1 nuclease digestion in denaturing conditions.

Chemical Mapping. DMS was used to modify adenosine and cytidine; kethoxal was used to modify guanosine; and CMCT was used to modify uridine. Chemical mapping of 5S rRNA was performed according to a published procedure (*34*), with several changes.

The salt dependence of reactivity of DMS on adenosine and cytosine and of CMCT on uridine was tested in buffers 1Na$^+$/4Mg^{2+}/10T, 0.04Na$^+$/10Mg^{2+}/10T, and 1Na$^+$/250T. Uridine (409 μM) in buffer was reacted with 102 mM CMCT for 15 min at room temperature. Adenosine (657 μM) and cytosine (722 μM) were reacted with 359 mM of DMS (3.9 μL of DMS in 10 μL of ethanol added to 100 μL of nucleoside solution) for 48 h at 37 °C. Reactions were stopped by freezing at −80 °C. Results were analyzed by high-performance liquid chromatography (HPLC). The extent of the reaction was typically between 30 and 50% and was independent of the buffer composition.

For chemical mapping, 2 pmol of 5S rRNA was taken for each reaction and annealed in buffers 1Na$^+$/4Mg^{2+}/10T or 0.04Na$^+$/10Mg^{2+}/10T, as described above. Then, tRNA carrier was added to give a total RNA concentration of 8 μM, and the solution was incubated for 10 min at the temperature of chemical mapping. Form B of 5S rRNA was prepared for chemical mapping as described above, and modification reactions were performed in buffer 1Na$^+$/250T

[1] Abbreviations: HPLC, high-performance liquid chromatography; DMS, dimethyl sulfate; CMCT, 1-cyclohexyl-3-(2-morpholinoethyl)-carbodiimide metho-*p*-toluenesulfonate; NMIA, *N*-methylisatoic anhydride.

at 4 °C. To a 9 μL sample, 1 μL of dimethyl sulfate or kethoxal solution was added. Dimethyl sulfate was diluted in ethanol and used at final concentrations of 60, 30, and 15 mM. Kethoxal was diluted in ethanol/water (1:3, v/v) to give final concentrations of 320, 160, and 80 mM. After modification with kethoxal, 3 μL of 35 mM sodium borate solution was added to stabilize products of modification. For modification with CMCT, 9 μL of CMCT solution was added to the 9 μL sample of RNA. CMCT was diluted in appropriate buffer (1Na^+/4Mg^{2+}/10T, 0.04Na^+/10Mg^{2+}/10T, or 1Na^+/250T) to give final concentrations in the reaction mixture of 625 (room temperature) or 500 (4 °C), 250, and 100 mM. Chemical modification reactions were performed for 20 min for chemical mapping at room temperature and 1.5 h for mapping at 4 °C. Reactions were stopped by ethanol precipitation on dry ice.

Chemical mapping was also done with *N*-methylisatoic anhydride (NMIA) according to a published procedure (*33*, *35*), with some changes. For each reaction, 2 pmol of 5S rRNA was annealed in buffers 1Na^+/4Mg^{2+}/10T, 0.15Na^+/4Mg^{2+}/10T, or 0.04Na^+/10Mg^{2+}/10T as described above. To a 9 μL sample, 1 μL of NMIA solution (1 or 0.5 mg of NMIA/42 μL of DMSO) was added. Samples were incubated for 3 h at room temperature. Reactions were stopped by ethanol precipitation on dry ice.

Primer Extension Reactions. DNA primers for primer extension reactions were 5′-ATGCCTGGCAGTTCCCT-3′ and 5′-GCGCTACGGCGTTTCAC-3′, which are complementary to nucleotides 104−120 and 54−70 of 5S rRNA, respectively. Primers were labeled on the 5′ end with [γ-^{32}P]-ATP according to the standard procedure. For each reaction, 2 pmol of primer was used. Primer extension was performed at 55 °C with reverse transcriptase SuperScript III and the buffers and protocol of Invitrogen. Reactions were stopped by adding loading buffer containing dye (Bromophenol Blue) and chilling to 0 °C. Products were separated on a 12% polyacrylamide denaturing gel. The gels were analyzed with the ImageQuant 5.2 program, and products were identified by comparing to sequencing lanes for A, C, T, and G and to control lanes. Modifications were initially identified by visual inspection of autoradiograms and were considered strong or medium when the band corresponding to the chemical modification had at least 6 or 2−6 times, respectively, the integrated intensity of the equivalent band in the control lane, as quantified with ImageQuant 5.2.

Preparation of Microarrays. Microarrays were prepared on agarose-coated slides according to the method described by Afanassiev et al. (*36*). Silanized slides were coated with 1% agarose activated by $NaIO_4$. On dried microarrays, 0.5 μL of 100 μM of each probe was spotted and incubated for 4 h at 37 °C in a 100% humidity chamber. The remaining aldehyde groups on microarrays were reduced with 35 mM $NaBH_4$ solution in PBS buffer and ethanol (3:1, v/v). Then, slides were washed in water at room temperature (3 washes for 30 min each), in 1% SDS solution at 55 °C for 1 h, and finally in water at room temperature (3 washes for 30 min each) and dried at room temperature overnight.

Hybridization Conditions. E. coli 5S rRNA was radioactively labeled with [^{32}P]Cp on the 3′ end according to the standard procedure and purified on an 8% polyacrylamide denaturing gel. For hybridization, labeled 5S rRNA was used at approximately 0.01 μM. Prior to hybridization, 5S rRNA was refolded as described above. Hybridization was performed in the same buffers used for folding. For hybridization, 200 μL of hybridization buffer containing target 5S rRNA was placed in a probe-clip press seal incubation chamber and incubated for 18 h at room temperature or 4 °C. At least 4 h was required to see strong signals, and 18 h was optimal. After hybridization, buffers with 5S rRNA were poured out and slides were washed in buffers with the same salt concentrations for 1 min at 0 °C. Then, slides were dried by slow centrifugation in a clinical centrifuge and covered with saran wrap. Hybridization was visualized by exposure to a phosphorimager screen, which was then scanned on a Molecular Dynamics 840 Storm Phosphorimager. Quantitative analysis was done with ImageQuant 5.2 software. Binding was considered strong when the integrated intensity was $\geq 1/3$ of the strongest integrated intensity for a given condition. Medium binding had integrated intensity from $1/3$ to $1/7$ of the strongest.

Ribonuclease H Assays. The 5S rRNA (4 pmol) was folded in buffer 0.15Na^+/4Mg^{2+}/10T, and then, a 10-fold excess of appropriate DNA oligomer in buffer 0.15Na^+/4Mg^{2+}/10T was added at room temperature to give a final DNA concentration of about 70 μM. The mixture was incubated for 1 h at room temperature. Then, DTT to a final concentration of 1 mM and 1.25 units of RNAsin and 1.3 units of ribonuclease H were added. The reaction was incubated for 20 min at room temperature. The reaction mixture was extracted twice with equal volumes of phenol/chloroform/isoamyl alcohol (25:24:1) (Aldrich). The residual phenol was removed by two chloroform extractions, and the RNA was precipitated with ethanol. Primer extension was used to identify sites of ribonuclease H cleavages.

Thermodynamic Measurements. Oligonucleotides were melted in a buffer containing 100 mM NaCl, 20 mM sodium cacodylate, and 0.5 mM Na_2EDTA at pH 7.0. Absorbance versus temperature melting curves were measured at 260 nm with a heating rate of 1 °C/min from 0 to 90 °C on a Beckman DU 640 spectrometer with a water-cooled Peltier thermoprogrammer. Melting curves were analyzed, and thermodynamic parameters were calculated with MeltWin 3.5 (*37*). Optical melting curves for 5S rRNA were measured in the same way, except that the RNA was first folded as described above.

RESULTS

Chemical Mapping of 5S rRNA from E. coli. The secondary structure of 5S rRNA was chemically mapped under several conditions (Figure 1): (A) buffer 1Na^+/4Mg^{2+}/10T at room temperature; (B) buffer 0.04Na^+/10Mg^{2+}/10T at room temperature, which is known to fold 5S rRNA into native form A (*25*); (C) buffer 1Na^+/4Mg^{2+}/10T at 4 °C; and (D) buffer 1Na^+/250T at 4 °C, which is used for probing form B. Native gel electrophoresis of 5S rRNA gave a single band for folding in each buffer.

The chemical reagents can modify nucleotides that are not in Watson−Crick pairs flanked by Watson−Crick pairs (*33*, *38*, *39*). Thus, the modifications in buffers 1Na^+/4Mg^{2+}/10T and 0.04Na^+/10Mg^{2+}/10T are consistent with the native structure A of 5S rRNA from *E. coli*, but in buffer 1Na^+/250T, the modifications of A29 and U32 are not consistent with the native structure A (Figure 1). The modifications in

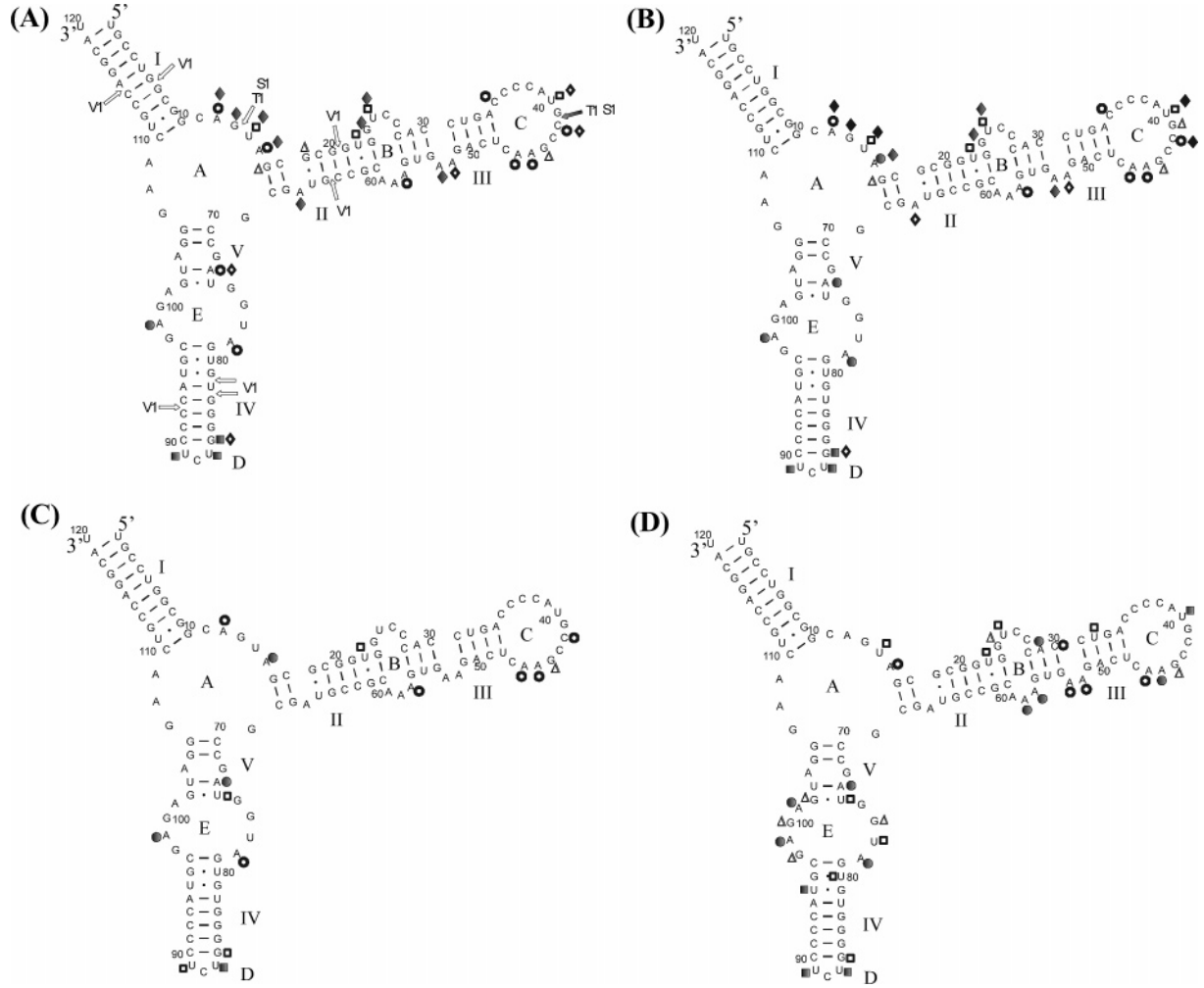

FIGURE 1: Chemical-mapping results. Conditions are (A) $1Na^+/4Mg^{2+}$/10T (1 M NaCl, 4 mM $MgCl_2$, and 10 mM Tris-HCl at pH 7.43), room temperature; (B) $0.04Na^+/10Mg^{2+}$/10T (40 mM NaCl, 10 mM $MgCl_2$, and 10 mM Tris-HCl at pH 7.43), room temperature; (C) $1Na^+/4Mg^{2+}$/10T (1 M NaCl, 4 mM $MgCl_2$, and 10 mM Tris-HCl at pH 7.43), 4 °C; and (D) $1Na^+$/250T (1 M NaCl and 250 mM Tris-HCl at pH 7.8), 4 °C. Also shown are results from nuclease mapping under condition A. Nucleases V1 and S1 are specific for double- and single-stranded regions, respectively. T1 is specific for single-stranded G. Symbols: ●, strong DMS; ○, medium DMS; ■, strong CMCT; □, medium CMCT; ▲, strong kethoxal; △, medium kethoxal; ◆, strong NMIA; ◇, medium NMIA.

buffer $0.04Na^+/10Mg^{2+}$/10T are consistent with those reported previously under similar conditions (*26*, *40*−*42*).

Although the modifications in buffers $1Na^+/4Mg^{2+}$/10T and $0.04Na^+/10Mg^{2+}$/10T are consistent with the native structure A of 5S rRNA from *E. coli*, the reactivities are buffer-dependent. In particular, in buffer $1Na^+/4Mg^{2+}$/10T at room temperature (Figure 1A), there are medium instead of strong DMS modifications of A15, A73, and A78, an additional medium kethoxal modification of G18, medium instead of strong NMIA modifications at U40 and C42, lack of modification of G41, and strong and medium NMIA modifications at A66 and A73, respectively, instead of a medium and no modification. Evidently, there are subtle changes in folding that are dependent upon NaCl and $MgCl_2$ concentrations. It is unlikely that these differences reflect any significant change in stability of secondary structure, however. Optical melting curves showed that the melting temperatures of the first transition were 54.9, 64.8, and 67.7 °C in buffer $1Na^+/4Mg^{2+}$/10T, $0.15Na^+/4Mg^{2+}$/10T, and $0.04Na^+/10Mg^{2+}$/10T, respectively. All are more than 30 °C higher than the temperature of the chemical-mapping experiments; therefore, the secondary structure is very stable in the presence of Mg^{2+}. Thus, the differences in chemical reactivity suggest only subtle changes in folding that are dependent upon NaCl and $MgCl_2$ concentrations.

Figure 1C shows chemical-mapping results in buffer $1Na^+/4Mg^{2+}$/10T at 4 °C. In comparison with room temperature (Figure 1A), there are fewer reactive bases, but the general pattern of modifications is very similar. Evidently, the secondary structure of 5S rRNA in buffer $1Na^+/4Mg^{2+}$/10T is close or identical to form A at room temperature and 4 °C, but there are subtle differences in local folding.

The structure of 5S rRNA in buffer $1Na^+/4Mg^{2+}$/10T at room temperature was also probed by enzymatic mapping. As shown in Figure 1A, the results are consistent with the secondary structure of form A. The results also agree with those in the literature under different buffer conditions giving form A (*26*, *27*, *40*, *41*).

Native gel electrophoresis of *E. coli* 5S rRNA in buffer $1Na^+$/250T gave a single band that migrated faster than the band of form A. In comparison to other conditions, many more chemical modifications were observed in buffer $1Na^+$/250T at 4 °C (see Figure 1D). The structure in buffer $1Na^+$/250T is clearly different from that in the other buffers.

Probing Form A of 5S rRNA from E. coli with Microarrays of 2′-O-Methylated Heptamers. Form A of 5S rRNA from

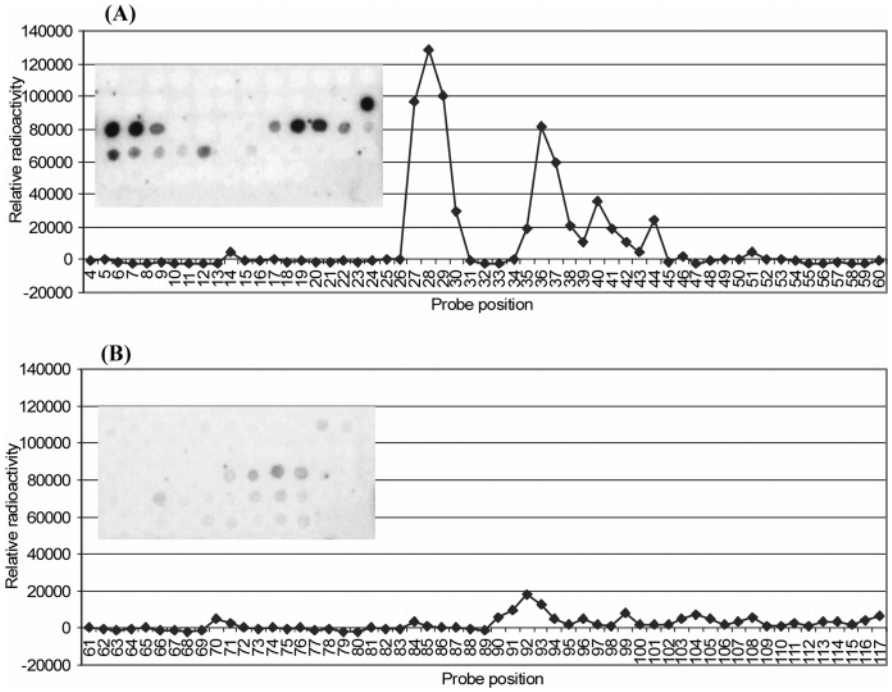

FIGURE 2: Hybridization results on 2′-*O*-methyl heptamer microarrays for 5S rRNA from *E. coli* in buffer $1Na^+/4Mg^{2+}$/10T (1 M NaCl, 4 mM $MgCl_2$, and 10 mM Tris-HCl at pH 7.43), room temperature. On microarrays shown, the 2′-*O*-methyl heptamers from left to right are (A) row 1, 4 → 15 (no binding detected); row 2, 16 → 27; row 3, 28 → 39; row 4, 40 → 51; row 5, 52 → 60 (no binding detected); (B) row 1, 61 → 72 (no binding detected); row 2, 73 → 84 (no binding detected); row 3, 85 → 96; row 4, 97 → 108 (no binding detected); row 5, 109 → 117 (no binding detected).

E. coli was probed under different conditions with microarrays having all possible complementary 2′-*O*-methylated RNA heptamers (Figures 2 and 3, Table 1, and the Supporting Information). Each 2′-*O*-methylated RNA heptamer is identified by a number corresponding to the number of the 5S rRNA nucleotide in the middle of the 5S rRNA sequence completely complementary to the heptamer probe.

The best discrimination between binding and nonbinding probes was achieved in buffer $1Na^+/4Mg^{2+}$/10T at room temperature (Figures 2 and 3 and Table 1). There was strong binding of probes 27−29, 36, and 37 and medium binding of probes 30, 35, 38/93 (which have the same sequence), 40, 41, 44, and 92. Similar relative binding was observed in buffers $0.15Na^+/4Mg^{2+}$/10T and $0.04Na^+/10Mg^{2+}$/10T at room temperature, but generally, the binding was weaker (see the Supporting Information). The strongest signal in buffers $0.15Na^+/4Mg^{2+}$/10T and $0.04Na^+/10Mg^{2+}$/10T was 4-fold weaker than in buffer $1Na^+/4Mg^{2+}$/10T. Evidently, the secondary structure of 5S rRNA in buffers $1Na^+/4Mg^{2+}$/10T, $0.15Na^+/4Mg^{2+}$/10T, and $0.04Na^+/10Mg^{2+}$/10T is the same at room temperature (form A), but the interactions between 5S rRNA and the probes are weaker in buffers $0.15Na^+/4Mg^{2+}$/10T and $0.04Na^+/10Mg^{2+}$/10T than in buffer $1Na^+/4Mg^{2+}$/10T.

The hybridization of 5S rRNA from *E. coli* to heptamer probes on microarrays was also studied in buffers $1Na^+/4Mg^{2+}$/10T, $0.15Na^+/4Mg^{2+}$/10T, and $0.04Na^+/10Mg^{2+}$/10T at 4 °C (Table 1 and the Supporting Information). Hybridization patterns and amplitudes at 4 °C change relative to room temperature. Usually, stronger binding is observed at 4 °C. The binding patterns for buffers $0.15Na^+/4Mg^{2+}$/10T and $0.04Na^+/10Mg^{2+}$/10T at 4 °C were similar to buffer $1Na^+/4Mg^{2+}$/10T at 4 °C (see the Supporting Information), but the strongest binding signal was 4-fold weaker.

The 4-fold difference between the maximum signal intensity in buffer $1Na^+/4Mg^{2+}$/10T and in buffers $0.15Na^+/4Mg^{2+}$/10T and $0.04Na^+/10Mg^{2+}$/10T shows that the concentration of NaCl is important and hybridization is optimized at 1 M NaCl. The melting temperature of polymer duplexes in the presence of Mg^{2+} is reduced as Na^+ is added (*43*, *44*), and this was also observed for optical melting curves of *E. coli* 5S rRNA, as mentioned above. Perhaps oligomer−polymer duplexes behave differently and/or the reduced stability of the tertiary structure of 5S rRNA in 1 M Na^+ facilitates binding to oligonucleotides.

Scanning for Alternative Binding Sites with the RNAstructure Program. There are only 16 384 heptamers with different sequences, and heptamer duplexes can be stable even when containing a mismatch. Thus, it is possible for a given heptamer to have more than one binding site on an RNA. The RNAstructure 4.11 program (*13*) was used in bimolecular folding mode to predict the formation of stable duplexes between unstructured *E. coli* 5S rRNA and probe oligonucleotides. The calculation of alternative binding sites included stability increments from mismatches and dangling ends. For *E. coli* 5S rRNA, probes 16 and 67, 38 and 93, and also 39 and 94 have identical sequences and thus have two completely complementary binding sites. Mismatched binding with free energy more favorable than −9 kcal/mol at 37 °C to completely unfolded 5S rRNA was also considered a possible alternative binding site. This corresponds to a dissociation constant of about 0.5 μM, which is 50-fold higher than the roughly 0.01 μM concentration of 5S rRNA on the microarray. Calculations by RNAstructure 4.11 are restricted to 37 °C and assume that both nucleic acid strands are not immobilized before binding, however, so that the predictions will underestimate binding to an immobilized strand at room temperature. These calculations

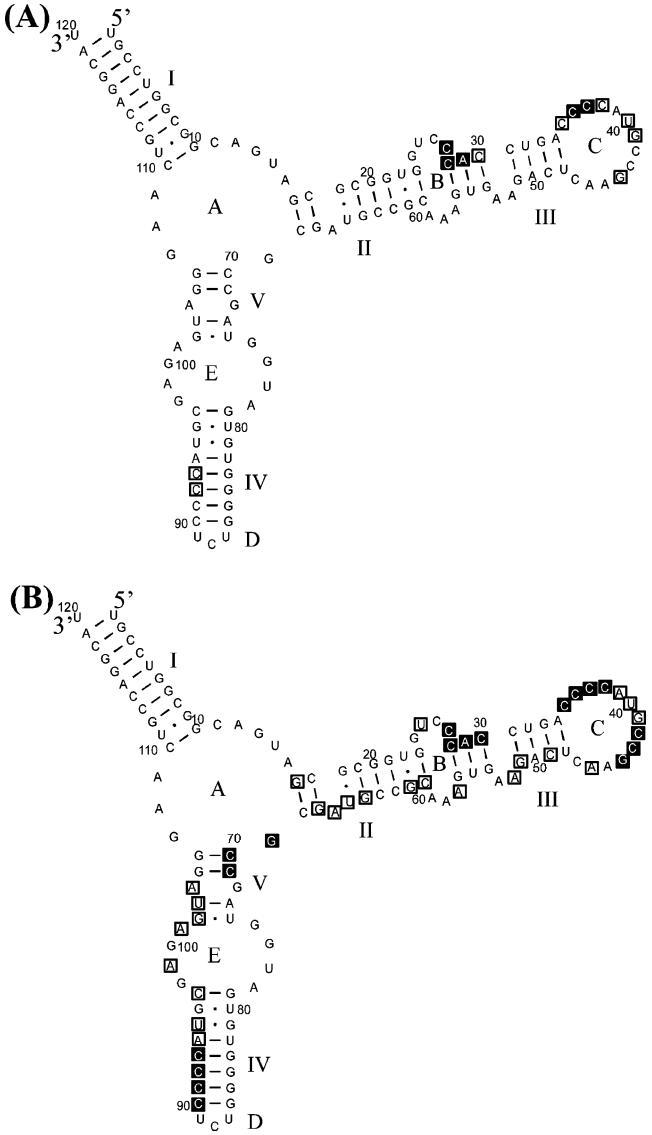

FIGURE 3: Hybridization results for 5S rRNA on 2′-*O*-methyl heptamer microarrays. Conditions are (A) $1Na^+/4Mg^{2+}$/10T (1 M NaCl, 4 mM $MgCl_2$, and 10 mM Tris-HCl at pH 7.43), room temperature; (B) $1Na^+$/250T (1 M NaCl and 250 mM Tris-HCl at pH 7.8), 4 °C. Note that probes 16 and 67, 38 and 93, and also 39 and 94 have identical sequences and that probe 92 likely binds to loop C. Symbols: ■ with text inside, middle site of strong binding; □ with text inside, middle site of medium binding.

revealed several alternative binding sites. For example, probe 37 could bind tightly at position 92/93, and probes 91 and 92 could bind at positions 37 and 37/38, respectively. The identical sequences of probes 38/93 and 39/94 along with possible mismatch binding of probes 37, 91, and 92 suggest that binding of probes 37−39 and 91−94 is to either positions 37−39, 91−94, or both. As described below, experiments with ribonuclease H support the interpretation that binding is to positions 37−39.

Ribonuclease H Cleavage Assay. To test the hypothesis that some probes have multiple binding sites, a ribonuclease H assay in $0.15Na^+/4Mg^{2+}$/10T buffer at room temperature was used to determine the position of binding for probes 28, 29, 37, 39/94, 41, 43, 91, and 92. Because 2′-*O*-methylated oligoribonucleotides do not induce ribonuclease H cleavage of RNA (*45*, *46*), the DNA analogues were used. The results are listed in Table 1. Oligonucleotide 28 induces medium cleavage after A29, and oligonucleotide 29 induces medium cleavage after C30 and C31. Oligonucleotide 41 induces strong cleavage after A39, U40, and C42, and oligonucleotide 43 induces strong cleavage after C42, G44, and A45. These patterns correlate well with the expected binding that is fully complementary (Table 1).

Oligonucleotide 39 has the same sequence as 94, and both only bind 5S rRNA on microarrays under certain conditions (see the Supporting Information). The DNA analogue of 39/94 induces medium ribonuclease H cleavages only after A39, U40, and C42, corresponding to the binding site at position 39 (Table 1). Probes 38 and 93 have the same sequence and presumably also bind to loop C. Thus, it is likely that loop C is responsible for the binding observed for probes 91−94. Oligonucleotides 37, 91, and 92 did not induce ribonuclease H cleavages, however. All of these oligonucleotides have G_4 sequences, which probably form stable quadruplexes in solution (*47*−*49*), thus prohibiting binding to RNA. Clearly, the interpretation of microarray binding results must consider potential alternative binding sites. Selected assays with ribonuclease H can sometimes identify actual binding sites.

Comparisons to Predictions from the OligoWalk Program. The OligoWalk program (*50*) was used to predict the free energies at 37 °C for binding of probes to the accepted secondary structure of form A of 5S rRNA (Table 1 and the Supporting Information). The free energies for breaking the target structure and binding probe to target RNA were only considered. The possibility of intermolecular association of probes was omitted because the probes are immobilized. The 2′-*O*-methylated heptamers were assumed to have the same energetics as RNA, which is consistent with optical melting studies on a series of 37 heteroduplexes (*51*).

With the exception of probe 30, oligonucleotides that bind strongly or moderately at room temperature are always predicted to have a ΔG°_{37} for hybridization to form A of *E. coli* 5S rRNA that is more favorable than −5 kcal/mol, although some of these favorable sites form mismatches and/or overhangs with the probe. For example, probe 92 has a predicted ΔG°_{37} that is unfavorable for binding at its fully complementary site but has a predicted favorable ΔG°_{37} of −10.3 kcal/mol for binding at position 38 (see Table 1). Probe 30 can bind more favorably at site 29 than at site 30 but still has a predicted ΔG°_{37} less favorable than −3 kcal/mol after allowing for the breaking of the target structure. Perhaps probe 30 binds to site 29 with coaxial stacking to flanking helixes. Coaxial stacking is not included in the OligoWalk algorithm but is favorable for duplex formation (*52*).

Binding to Shorter Versions of the Probe Reveals the Number of Base Pairs Required for Binding at a Particular Site. As a test of the number of base pairs required to observe binding, the binding was measured to sequentially shortened versions of probe 35, 5′-$G^MG^MG^MG^MU^MC^MA^M$, which strongly and moderately binds 5S rRNA at 4 °C and room temperature, respectively. In buffer $1Na^+/4Mg^{2+}$/10T at 4 °C, probes 5′-$G^MG^MG^MG^MU^MC^M$, 5′-$G^MG^MG^MG^MU^M$, and 5′-$G^MG^MG^MG^M$ gave signals with 0.8, 0.6, and 0.4 times the intensity of probe 35, respectively. In contrast, hexamer 5′-$G^MG^MG^MU^MC^MA^M$ gave only 0.1 times the intensity of probe 35, and 5′-$G^MG^MU^MC^MA^M$ and 5′-$G^MU^MC^MA^M$ gave no signal. At room temperature, 5′-$G^MG^MG^MG^MU^MC^M$ gave 0.4 times

Table 1: Hybridization Results in 1 M NaCl, 4 mM $MgCl_2$, and 10 mM Tris-HCl at pH 7.43 ($1Na^+/4Mg^{2+}$/10T), RNAstructure Calculations, and Ribonuclease H Cleavages[a]

center of binding site	sequence of probe (5′−3′)	5S rRNA binding 4 °C	5S rRNA binding RT	$\Delta G°_{37}$ predicted (kcal/mol) break local structure of 5S rRNA	$\Delta G°_{37}$ predicted (kcal/mol) no structure of 5S rRNA	alternative binding site	$\Delta G°_{37}$ predicted (kcal/mol) for alternative binding site (no structure of 5S rRNA)	sites of ribonuclease H cleavage
27	GUGGGAC	S	S	−9.1	−12.2	−	−	
28	GGUGGGA	S	S	−7.2	−13.4	−	−	M A29
29	AGGUGGG	S	S	−5.4	−12.5	−	−	M C30 M C31
30	CAGGUGG	M	M	−1.0	−12.4	29/30	−9.9	
35	GGGGUCA	S	M	−6.3	−13.8	−	−	
36	UGGGGUC	S	S	−7.8	−12.6	−	−	
37	AUGGGGU	S	S	−10.0	−11.3	92/93	−9.9	−
38/93	CAUGGGG	M	M	−11.1	−12.0	93	−11.6	
39/94	GCAUGGG	−	−	−11.2	−12.3	94	−13.2	M A39 M U40 M C42
40	GGCAUGG	S	M	−11.2	−13.2	94/95	−9.9	
41	CGGCAUG	M	M	−10.3	−11.7	−	−	S A39 S U40 S C42
42	UCGGCAU	S	−	−10.6	−10.7	71	−9.2	
43	UUCGGCA	M	−	−10.4	−10.2	71	−9.4	S C42 S G44 S A45
44	GUUCGGC	M	M	−10.5	−11.7	−	−	
70	UCGGCGC	M	−	−4.6	−13.5	(1) 42/43 (2) 62	(1) −9.4 (2) −9.2	
71	AUCGGCG	M	−	−2.9	−11.3	42/43	−9.4	
90	GGGGAGA	M	−	0.2	−14.1	−	−	
91	UGGGGAG	S	−	2.3	−12.6	37	−9.1	−
92	AUGGGGA	S	M	2.9	−11.2	37/38	−10.3	−
93/38	CAUGGGG	M	M	5.1	−11.6	38	−12.0	
94/39	GCAUGGG	−	−	6.5	−13.2	39	−12.3	M A39 M U40 M C42

[a] Each 2′-*O*-methylated RNA heptamer is identified by the number corresponding to the number of the 5S rRNA nucleotide complementary to the middle nucleotide of the heptamer probe (center of the binding site). Alternative binding sites are defined by the middle nucleotide of the binding region on 5S rRNA. S = strong binding (from 1 to $^1/_3$ integrated intensity of the strongest integrated intensity in a given condition). M = medium binding (from $^1/_3$ to $^1/_7$ integrated intensity of the strongest). Ribonuclease H cleavage occurs 3′ of the nucleotides listed in the right most column. "−" indicates that the probe does not bind or ribonuclease H does not cleave. The predicted values of $\Delta G°_{37}$ for 5S rRNA with no structure include contributions from the first 5′ and 3′ dangling ends, which sometimes results in more favorable binding to alternative binding sites relative to sites fully complementary to the probe.

the intensity of probe 35, but the other shortened probes gave no signal. Evidently, only the four consecutive GC pairs are required for binding of probe 35 at 4 °C, but at least six base pairs are required for binding at room temperature.

Probe 90, 5′-$G^MG^MG^MG^MA^MG^MA^M$, binds *E. coli* 5S rRNA in buffers $1Na^+/4Mg^{2+}$/10T, $0.15Na^+/4Mg^{2+}$/10T, and $0.04Na^+/10Mg^{2+}$/10T at 4 °C (Table 1 and the Supporting Information). Further insight into this binding was provided by shorter probes 5′-$G^MG^MG^MA^MG^MA^M$ and 5′-$G^MG^MA^MG^MA^M$. Neither probe binds to 5S rRNA at 4 °C in any of the three buffers. These results, together with those for 5′-$G^MG^MG^MG^M$, which binds with 0.5 times the intensity of probe 90, are consistent with probe 90 binding only to loop C. The results suggest that a comparison between possible secondary structures and binding of different length oligonucleotides can help identify correct structures. A related approach was used with equilibrium dialysis data (*15*).

Binding of Form B of E. coli 5S rRNA to Microarrays. The 5S rRNA was folded into form B as described in the Materials and Methods, and hybridization was performed in buffer $1Na^+$/250T at 4 °C to avoid refolding into form A during hybridization. Many more probes bound in buffer $1Na^+$/250T than in buffers giving form A (see Figure 3). Evidently, oligonucleotide binding to *E. coli* 5S rRNA is facilitated by the absence of Mg^{2+}.

Application of Probes Containing 2-Thiouridine To Enhance Stability of A−U Pairs and Discrimination between A−U and G−U Pairs. Two problems that arise in interpretation of oligonucleotide-binding data are the sequence dependence of stabilities for perfectly matched helixes and the stabilities of helixes with non-Watson−Crick pairs. The sequence dependence of stabilities is illustrated by the predicted range of $\Delta G°_{37}$ from −6 to −15 kcal/mol for binding of the heptamers to their unfolded heptamer complements (see Table S1 in the Supporting Information). This corresponds to over a million-fold range in the binding constant. The problem of non-Watson−Crick pairs is most acute for G−U pairs because they have stabilities similar to A−U pairs (*7*, *9*, *53*). Modified nucleotides provide one way to achieve more uniform and specific binding of probes to target RNA. For example, 2-thiouridine enhances the thermodynamic stability of A−U pairs (*54*−*57*). In the RNA/RNA duplex, 5′-GAGUGAG/3′-CUCACUC, 2-thiouridine stabilizes the middle A−U pair by 1.1 kcal/mol and destabilizes the corresponding G−U pair by 0.3 kcal/mol at 37 °C (*57*). To test this in RNA/2′-*O*-methyl RNA hybrids,

Table 2: Thermodynamic Parameters of Heteroduplexes of RNA and 2′-*O*-Methyl Oligoribonucleotides[a]

duplexes			average of curve fits				T_M^{-1} versus log C_T plots					
	RNA	2′-*O*-MeRNA	$-\Delta H°$ (kcal/mol)	$-\Delta S°$ (eu)	$-\Delta G°_{37}$ (kcal/mol)	T_M[b] (°C)	$-\Delta H°$ (kcal/mol)	$-\Delta S°$ (eu)	$-\Delta G°_{37}$ (kcal/mol)	T_M[b] (°C)	$\Delta\Delta G°_{37}$[c] (kcal/mol)	ΔT_M[b,c] (°C)
Probe 40 Mimics												
A−U	5′-CC**A**UGCC	5′-GGCA**U**GG	69.1 ± 2.5	190.9 ± 7.7	9.86 ± 0.13	52.7	64.1 ± 3.1	175.6 ± 9.6	9.69 ± 0.11	53.1		
A−s^{2}U	5′-CC**A**UGCC	5′-GGCA**s^{2}U**GG	75.1 ± 13.5	206.2 ± 40.6	11.16 ± 0.90	57.4	83.1 ± 13.8	230.6 ± 41.8	11.56 ± 0.87	57.0	−1.87	3.9
G−U	5′-CC**G**UGCC	5′-GGCA**U**GG	61.5 ± 2.2	173.1 ± 7.1	7.78 ± 0.05	43.4	58.4 ± 1.6	163.2 ± 4.9	7.76 ± 0.01	43.7		
G−s^{2}U	5′-CC**G**UGCC	5′-GGCA**s^{2}U**GG	61.1 ± 3.7	171.9 ± 11.9	7.80 ± 0.07	43.6	56.9 ± 4.02	158.6 ± 12.7	7.73 ± 0.09	43.7	+0.03	0
C → U in Probe 40												
A−U	5′-CCAU**A**CC	5′-GG**U**AUGG	64.7 ± 2.1	181.4 ± 6.8	8.41 ± 0.06	46.3	57.2 ± 2.7	157.4 ± 8.7	8.34 ± 0.04	47.2		
A−s^{2}U	5′-CCAU**A**CC	5′-GG**s^{2}U**AUGG	65.1 ± 3.3	179.9 ± 10.3	9.27 ± 0.19	50.6	58.8 ± 0.9	160.5 ± 2.9	9.05 ± 0.03	50.9	−0.71	3.7
G−U	5′-CCAU**G**CC	5′-GG**U**AUGG	77.9 ± 17.3	231.2 ± 56.1	6.19 ± 0.10	35.7	69.6 ± 4.2	204.5 ± 13.9	6.22 ± 0.08	35.6		
G−s^{2}U	5′-CCAU**G**CC	5′-GG**s^{2}U**AUGG	76.9 ± 14.7	229.1 ± 47.7	5.80 ± 0.07	34.1	77.9 ± 8.6	232.6 ± 27.9	5.82 ± 0.13	34.2	+0.40	−1.7
Probe 56 Mimics												
A−U	5′-**A**GUGA**AA**	5′-**UUU**CAC**U**	59.7 ± 6.7	177.7 ± 22.6	4.60 ± 0.35	27.3	56.4 ± 3.5	166.3 ± 11.9	4.79 ± 0.16	27.7		
A−s^{2}U	5′-**A**GUGA**AA**	5′-**Us^{2}U**UCA**Cs^{2}U**	53.9 ± 8.0	154.4 ± 25.8	6.07 ± 0.13	34.4	48.5 ± 6.5	136.7 ± 21.4	6.11 ± 0.30	34.3	−1.32	6.6
A−s^{2}U	5′-**A**GUG**AAA**	5′-**s^{2}UUs^{2}U**CA**Cs^{2}U**	59.4 ± 3.8	169.8 ± 12.2	6.70 ± 0.06	37.9	54.5 ± 1.7	153.7 ± 5.6	6.77 ± 0.03	38.4	−1.98	10.7
A−s^{2}U	5′-**A**GUG**AAA**	5′-**s^{2}Us^{2}Us^{2}U**CA**Cs^{2}U**	64.5 ± 4.8	181.8 ± 15.4	8.10 ± 0.09	44.8	60.2 ± 1.6	168.1 ± 5.1	8.04 ± 0.02	45.0	−3.25	17.3

[a] Solutions are 100 mM NaCl, 20 mM sodium cacodylate, and 0.5 mM Na_2EDTA at pH 7. [b] Calculated for a 10^{-4} M oligonucleotide concentration. [c] Differences because of the substitution of U with s^{2}U.

5′-*O*-dimethoxytrityl-2′-*O*-methyl-2-thiouridine 3′-*O*-phosphoramidite (*58*) was synthesized and used for preparing model probes. Several RNA/2′-*O*-methyl RNA duplexes without the C6 aminolinker were melted, and thermodynamic parameters are collected in Table 2. The 2′-*O*-methylated probe 40, 5′-G^{M}G^{M}C^{M}A^{M}U^{M}G^{M}G^M, was chosen as a reference for duplex formation with natural bases. Probe 40 was selected because on microarrays at room temperature and 1 M NaCl it hybridized with medium strength to 5S rRNA and is expected to only hybridize to position 40. For the complementary duplex 5′-G^{M}G^{M}C^{M}A^{M}U^{M}G^{M}G^M/3′-CCGUACC in solution, the measured $\Delta G°_{37}$ is −9.69 kcal/mol and the T_m is 53.1 °C. When 2′-*O*-methyl uridine was replaced by 2′-*O*-methyl-2-thiouridine, the complementary duplex was stabilized by 1.87 kcal/mol and the T_m was increased by 3.9 °C. When the RNA was changed to 3′-CCGUGCC to form a G−U pair, the $\Delta G°_{37}$ was about −7.75 kcal/mol with either U or s^{2}U^M in the 2′-*O*-methyl strand. Thus, discrimination for A−U over G−U is enhanced by about 1.9 kcal/mol in this context.

The oligonucleotides, 5′-G^{M}G^{M}U^{M}A^{M}U^{M}G^{M}G^M and 5′-G^{M}G^{M}s^{2}U^{M}A^{M}U^{M}G^{M}G^M, were synthesized to test the effect of s^{2}U^M in another context. In this case, the duplex with the A−s^{2}U^M pair is 0.71 kcal/mol more stable than that with the A−U pair. The duplex with the G−s^{2}U^M pair is less stable by 0.40 kcal/mol relative to the duplex with a G−U pair (Table 2). Thus, discrimination for A−U over G−U is enhanced by 1.1 kcal/mol at 37 °C in this context.

Preliminary microarray results demonstrated that 5′-G^{M}G^{M}C^{M}A^{M}s^{2}U^{M}G^{M}G^M exhibits strong binding of *E. coli* 5S rRNA in $1Na^+$/$4Mg^{2+}$/10T and $0.15Na^+$/$4Mg^{2+}$/10T at 4 °C and medium binding at room temperature, which is the same pattern observed for the unmodified probe 40. The mismatched probe 5′-G^{M}G^{M}s^{2}U^{M}A^{M}U^{M}G^{M}G^M does not bind under any of the conditions tested.

Various combinations of s^{2}U^M incorporated into probe 56, 5′-U^{M}U^{M}U^{M}C^{M}A^{M}C^{M}U^M, were also tested. Probe 56 is complementary to loop B but did not bind in microarray experiments. To determine if this was due to the large AU content and if s^{2}U^M substitution could enhance binding, the following oligomers were synthesized: 5′-U^{M}s^{2}U^M-U^{M}C^{M}A^{M}C^{M}s^{2}U^M, 5′-s^{2}U^{M}U^{M}s^{2}U^{M}C^{M}A^{M}C^{M}s^{2}U^M, and 5′-s^{2}U^{M}s^{2}U^{M}s^{2}U^{M}C^{M}A^{M}C^{M}s^{2}U^M. The thermodynamics of these probes and probe 56 binding to their RNA complement, 5′-AGUGAAA, were measured (Table 2).

Two 2′-*O*-methyl-2-thiouridines in probe 56 increase the stability of the duplex by 1.32 kcal/mol at 37 °C and the T_m by 6.6 °C. Three modifications increase the stability by 1.98 kcal/mol and T_m by 10.7 °C. Four s^{2}U^M nucleotides increase the stability by 3.25 kcal/mol, to give a $\Delta G°_{37}$ for duplex formation of −8.04 kcal/mol and a melting temperature of 45.0 °C, which is 17.3 °C higher than the duplex without modifications. On average, each 2′-*O*-methyl-2-thiouridine stabilized this RNA/2′-*O*-methyl RNA duplex by 0.7 kcal/mol. Thus, 2′-*O*-methyl-2-thiouridine stabilizes A−U^M pairs in RNA/2′-*O*-methyl RNA duplexes in a context-dependent manner.

The modified probe 56, 5′-s^{2}U^{M}s^{2}U^{M}s^{2}U^{M}C^{M}A^{M}C^{M}s^{2}U^M, was immobilized on microarrays. In buffer $1Na^+$/$4Mg^{2+}$/10T, this probe hybridized to *E. coli* 5S rRNA with medium and weak strength at 4 °C and room temperature, respectively. In buffer $0.15Na^+$/$4Mg^{2+}$/10T at 4 °C, it bound weakly. The unmodified probe did not bind under any conditions. Thus, 2′-*O*-methyl-2-thiouridine substitutions can enhance binding to microarrays.

Improving Secondary Structure Predictions by RNAstructure. One goal of this work is to improve secondary structure predictions by programs such as RNAstructure (*13*). Constraints from chemical mapping *in vivo* improve the prediction for *E. coli* 5S rRNA secondary structure from 26 to 87% accuracy (*13*). Using constraints from the *in vitro* chemical probing of form A 5S rRNA from this work, the predicted lowest free-energy structure has 100% of the known base pairs. This was found separately for constraints from buffer $1Na^+$/$4Mg^{2+}$/10T at room temperature or at 4 °C or from buffer $0.04Na^+$/$10Mg^{2+}$/10T at room temperature. No constraints from NMIA reactivity were included in these calculations because the rules for NMIA reactivity have not been fully determined yet.

Microarray data may be used as constraints if the middle nucleotide of probes with clear binding sites is treated the same as a site of chemical modification. Data from hybridization of 5S rRNA at room temperature were chosen for this approach because of better discrimination against

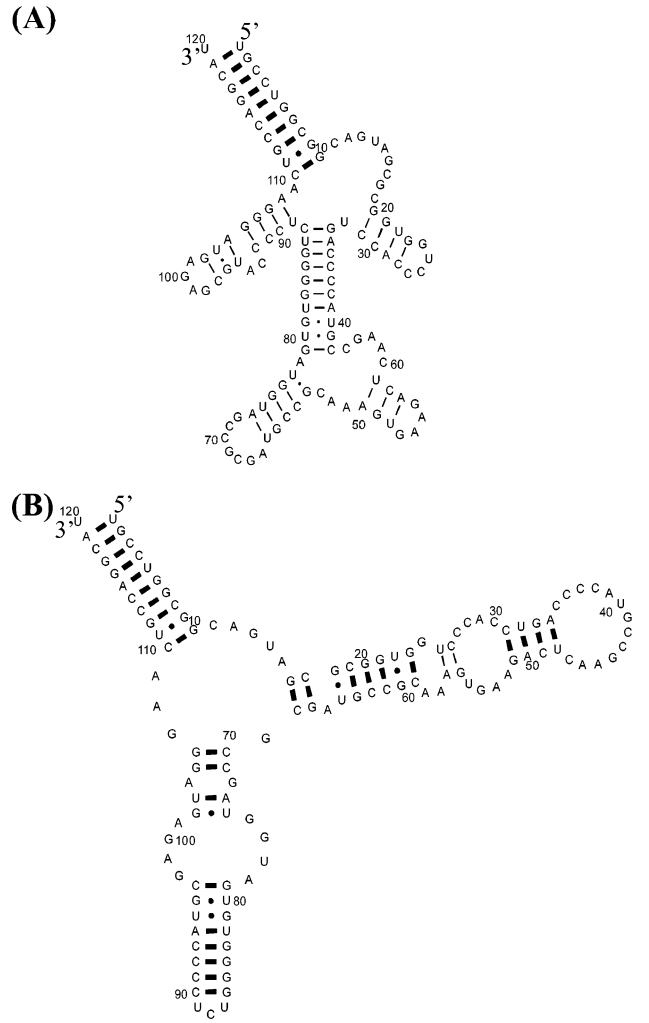

FIGURE 4: RNAstructure 4.11 prediction for *E. coli* 5S rRNA secondary structure (A) without constraints and (B) with constraints from hybridization results. Correct base pairs are bolded. Nucleotides constrained were (buffer $1Na^+/4Mg^{2+}$/10T) 27−29, 35, 36, 40, 41, 44; (buffer $0.15Na^+/4Mg^{2+}$/10T) 27−29, 35, 36, 39, 40, 44; and (buffer $0.04Na^+/4Mg^{2+}$/10T) 27−29, 35 36, 39, 40, 41, 44, 90. All three sets of constraints gave the same predicted structure.

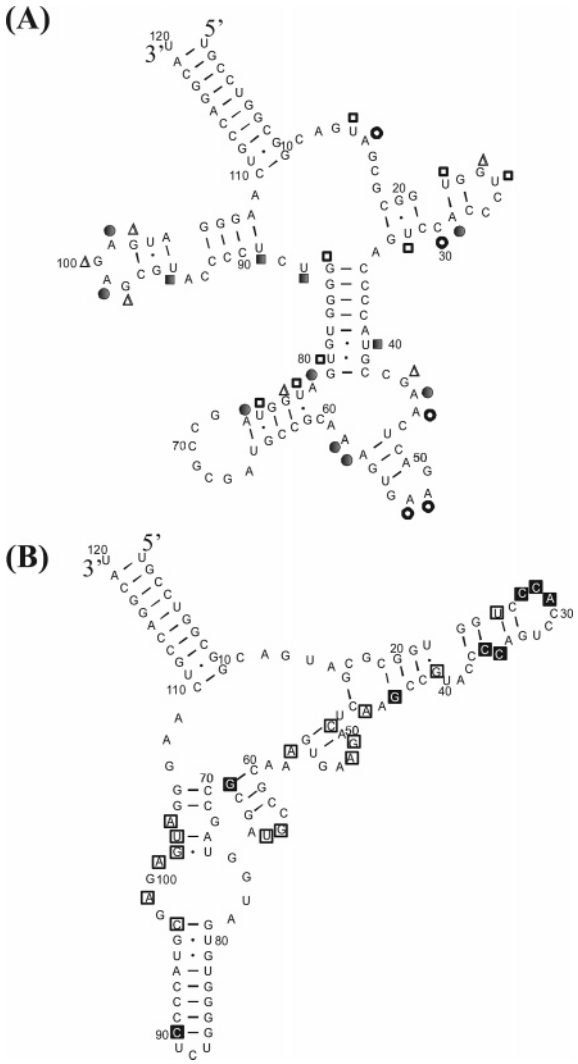

FIGURE 5: RNAstructure 4.11 predictions for form B of *E. coli* 5S rRNA in $1Na^+$/250T (1 M NaCl and 250 mM Tris-HCl at pH 7.8), 4 °C. (A) Using constraints from chemical-mapping data alone, $\Delta G°_{37} = -46.8$ kcal/mol, and (B) using constraints shown from oligonucleotide-binding data alone, $\Delta G°_{37} = -44.8$ kcal/mol. The structure shown in B is also predicted when both chemical-mapping and oligonucleotide-binding data are used as constraints. Note that all binding oligonucleotides shown in Figure 3 are not used as constraints because some have potential alternative binding sites (see Table S1 in the Supporting Information). Symbols: ●, strong DMS; ○, medium DMS; ■, strong CMCT; □, medium CMCT; ▲, strong kethoxal; △, medium kethoxal; ■ with text inside, middle site of strong binding; □ with text inside, middle site of medium binding.

mismatches. Probes with alternative binding sites were omitted from constraints if the probe completely complementary to the alternative binding site also bound 5S rRNA at least as strongly as the probe in question. An exception was made for probe 39 on the basis of ribonuclease H cleavages, indicating a single binding site for probe 39. The middle nucleotide of probes binding 5S rRNA with strong and medium intensity and which can bind tightly only by forming perfect duplexes were used as chemical modification constraints in predictions of secondary structure by RNAstructure 4.11 (see the caption to Figure 4). For each buffer, the lowest free-energy structure has 92% of the known canonical base pairs. As shown in Figure 4B, only part of helix III is predicted to be in an alternative fold. The crystal structure of 5S rRNA from *H. marismortui* has Watson−Crick base pairs with unusual geometries in this region (*24*), suggesting a pliable local structure.

The structure of form B was also predicted with RNAstructure 4.11. Constraints from chemical mapping and from hybridization in buffer $1Na^+$/250T were used separately and together (Figure 5). In all cases, the predicted lowest free-energy structure had a helix, which is also present in form A: U1−G10/C110−A119. Helix U1−G10/C110−A119 in both A and B forms is in agreement with proposed earlier structures (*25*, *28*). Helix C35−C42/G79−G86 appears when only chemical-mapping constraints are used (Figure 5A). The formation of helix G33−C42/G79−C88 (*25*) or G33−A39/U82−C88 (*28*) for form B was proposed previously. This helix is also consistent with V1 cuts in region G33−C42 (*27*). This secondary structure is not consistent, however, with the binding observed to oligonucleotides 36 and 90. When hybridization constraints alone or together with chemical-mapping constraints are used, the structure shown in Figure 5B is predicted. This structure is predicted to be only 2 kcal/mol less favorable than the structure in Figure 5A. This suggests that Figure 5B is a structure of form B. It

is possible that the two structures in Figure 5 and others are able to convert in the absence of Mg^{2+}. Form B exhibits many more sites of chemical modifications (Figure 1) and heptamer binding (Figure 3) as compared to form A. Perhaps the density of oligonucleotide-binding sites can provide insight into the rigidity of a structure.

DISCUSSION

In this paper, probing of secondary structure by microarrays of oligonucleotides is explored as an approach to improve the prediction of RNA secondary structure. Free-energy minimization typically predicts correctly only about 70% of known canonical base pairs (*7*). One way to improve modeling of RNA secondary structure is to couple computations with experimental data. For example, enzymatic (*34*, *59*) or chemical (*34*, *38*, *39*) mapping can reveal nucleotides that are not involved in canonical base pairs, and this information can be used as constraints in computations (*7*, *12*, *13*). We show here that hybridization on microarrays with heptamer 2′-*O*-methyl oligoribonucleotides can provide additional experimental constraints that allow the prediction of a nearly true secondary structure by a free-energy minimization algorithm. In principle, microarrays can interrogate RNA secondary structure in a way that is faster and more easily automated than chemical probing, while also providing complementary information. The general method should also be applicable to systems that are not amenable to chemical probing, e.g., any system that relies on complementary, noncovalent interactions for folding but does not have a backbone that allows readout by a polymerase of reactivity to chemicals.

The influence of the RNA structure on hybridization to microarrays was first studied by Mir et al. (*60*). They used DNA oligonucleotides with lengths of 2−12 nucleotides immobilized on a glass surface and $tRNA^{Phe}$ as the target. For probing of secondary structure, small probes have several advantages relative to longer probes. The first is better discrimination between Watson−Crick complementary binding and binding involving mismatches. The second is less possibility to disrupt secondary structure in the target. A third is that self-folding of the probe can be ignored. Moreover, there are only 16 384 possible heptamers; therefore, microarrays containing all possible heptamers could be mass-produced. Even a microarray containing all possible heptamers, hexamers, pentamers, and tetramers would have only 21 760 oligonucleotides. As demonstrated for probe 90, comparisons of relative binding by different length oligonucleotides can provide insight into secondary structure. The disadvantage of short oligonucleotides is less specificity, because long RNAs are likely to have multiple regions with the same sequence. Heptamers are expected to be ideal for probing the structures of RNAs shorter than roughly 1000 nucleotides because on average a given seven nucleotide sequence will be present twice only 6% of the time in a 1000 nucleotide sequence.

For this study, 2′-*O*-methyl RNA probes were selected because 2′-*O*-methyl RNA/RNA duplexes are thermodynamically more stable than DNA/RNA duplexes (*51*, *61*, *62*). Moreover, chemical synthesis of 2′-*O*-methylated oligoribonucleotides is efficient and inexpensive, and the oligonucleotides are chemically stable. Such 2′-*O*-methyl RNA probes have been used in microarrays previously (*61*) although not for probing structure.

E. coli 5S rRNA was used to test oligonucleotide probing of secondary structure because only 27% of its canonical base pairs are predicted correctly by free-energy minimization (*7*, *13*). This is likely due to unusual stabilization of loop E by about −8.8 and −5.0 kcal/mol relative to 0.1 and 1 M Na^+, respectively, when compared to 50 mM Mg^{2+} and 0.1 M Na^+ (*63*). Thus, *E. coli* 5S rRNA provides a good test of whether experimental data can compensate for incomplete knowledge of RNA thermodynamics.

Hybridization was tested in several buffers at room temperature and 4 °C. Chemical mapping showed that folding *E. coli* 5S rRNA in buffers $1Na^+/4Mg^{2+}$/10T, $0.15Na^+/4Mg^{2+}$/10T, or $0.04Na^+/10Mg^{2+}$/10T gave native form A. The best condition for hybridization experiments was buffer $1Na^+/4Mg^{2+}$/10T at room temperature. This condition gave both a high signal intensity and good discrimination against mismatches.

Binding of A Form E. coli 5S rRNA to Immobilized Oligonucleotides Is Consistent with the Known Secondary Structure. *E. coli* 5S rRNA binds to microarrays very similarly in buffers $1Na^+/4Mg^{2+}$/10T, $0.15Na^+/4Mg^{2+}$/10T, and $0.04Na^+/10Mg^{2+}$/10T (see the Supporting Information). Differences in intensity are mostly observed. The most accessible region for binding of probes was loop C. In buffer $1Na^+/4Mg^{2+}$/10T at room temperature, probes 35−38, 40, 41, and 44 hybridized to loop C (Figure 3A). Differences in the strength of binding and in chemical modification at positions in the loop may come from tertiary interactions. For example, extension of helix III by three noncanonical base pairs into loop C has been proposed (*41*). A crystal structure of the equivalent loop in the large ribosomal subunit from *H. marismortui* shows that this loop has a Watson−Crick pair between C38 and G44 as well as tertiary interactions between A39 and A46 and between U40 and A45 (*24*). Probes probably break some tertiary interactions to allow hybridization, but the free-energy cost is small. Experiments with truncated versions of probe 35 showed that it had to invade helix III to bind at room temperature but not at 4 °C.

The 5′ side of loop B is the only other region giving strong binding to probes in buffer $1Na^+/4Mg^{2+}$/10T (Figure 3A). Probes complementary to the 3′ side of loop B did not bind well, except for modified probe 56, 5′-$\underline{s^2U^M}$-$\underline{s^2U^Ms^2U^M}C^MA^MC^M\underline{s^2U^M}$, at 4 °C. This is likely due to the high AU content and therefore weak base pairing of probes binding to the 3′ side. Published experiments and a molecular dynamics study suggest lability of the helix III/loop B region (*25*, *64*, *65*). DNA analogues of probes 28 and 29 induce ribonuclease H cleavage between nucleotides 29−31, indicating that the base pairs in that region are labile. Thus, the structure shown in Figure 4B may be similar in stability to the known structure shown in Figure 3A. In the crystal structure of the large ribosomal subunit from *H. marismortui* (*24*), the base pairs equivalent to helix C28−C30/G54−G56 have unusual geometries. Perhaps a dynamic structure in that region is important for function.

E. coli 5S rRNA also bound to probes 92 and 93. The sequence of 93, however, is identical to 38, which is complementary to loop C. Probe 92 can form six complementary base pairs with loop C, having only a single A

dangling at the 3′ end. Thus, binding to probes 92 and 93 is consistent with native structure A.

Other regions of 5S rRNA did not bind to probes. The lack of binding to loop E is consistent with chemical mapping (*41*, *66*) and NMR (*22*) and crystal (*23*) structures of loop E, which show noncanonical base pairs: G72−A104, U74−G102, G75−A101, G76−G100, U77−A99, and A78−G98. Thermodynamic measurements in the presence of magnesium revealed unusual stability for loop E (*63*). NMR results also show that Mg^{2+} is required for forming a structured loop E (*22*). As shown in Figure 1, nucleotides in the "loop E" region are more reactive during chemical mapping in buffer $1Na^{+}$/250T, without magnesium. Thus, the microarray data showing that probes do not bind to loop E in the presence of Mg^{2+} are consistent with its known properties.

Microarray probes 12 and 14 did not bind to the multibranch loop, although binding is predicted by the OligoWalk program. A12, U14, and A15 were accessible to chemicals, however (Figure 1). This suggests that the multibranch loop is also more stable than predicted. Thermodynamic measurements have revealed extra stability for a 5S rRNA multibranch loop with a different sequence (*67*).

Microarray Data Provide New Insight into the Structure of Form B of E. coli 5S rRNA. Chemical mapping and hybridization to probes under conditions known to give form B of *E. coli* 5S rRNA gave results dramatically different from those under conditions giving form A. More regions are accessible for both chemical reaction and binding to microarray probes. Interestingly, the structure prediction with constraints from microarray data alone or from both microarray and chemical-mapping data suggests a secondary structure different from that generated when only chemical modification data are used as constraints (Figure 5). The presence of the strong helix U1−G10/C110−A119 in both structural models is consistent with previous suggestions, however (*25*, *28*). While a single structure is implied by the observation of a single band on a nondenaturing gel, it is possible that the absence of Mg^{2+} allows this structure to be more dynamic. A comparison of the microarray data for forms A and B (Figure 3) suggests that binding to microarrays may allow the identification of regions in an RNA that are particularly rigid or dynamic.

Substitution with 2-Thiouridine Can Enhance Binding and Specificity of 2′-O-Methyl Oligonucleotides. Interpretation of microarray data is potentially confounded by binding involving mismatches. The different stabilities of complementary duplexes formed by probes with different AU and GC contents may also limit the information content of microarray data. In principle, modified nucleotides can overcome these limitations. To illustrate this, 2′-O-methyl-2-thiouridine was tested to improve binding and discrimination in base pairing. As shown in Table 2, 2′-O-methyl-2-thiouridine substitutions enhance the stability of an A−U pair by an average of 0.8 kcal/mol of substitution at 37 °C. For the two cases tested, s^2U^M substitution also enhanced discrimination of A−U over G−U pairs by 1.1 and 1.9 kcal/mol. Preliminary results with microarrays suggest that 2′-O-methyl-2-thiouridine is a promising modification for microarray technology.

Interpretation of Binding to Microarrays Can Provide Insight into RNA Structure and Dynamics. Microarrays with all possible heptamers, hexamers, pentamers, and tetramers together with programs such as RNAstructure (*13*) can be a useful tool to deduce the secondary structure and dynamics of RNA. Microarrays rapidly interrogate oligonucleotide binding to an RNA. The bimolecular folding mode in RNAstructure can predict which probes that bind may also have more than one binding site including those with mismatches. These can still be used as constraints if the oligonucleotide fully complementary to the alternative binding site binds more weakly than the mismatched probe. Otherwise, probes with alternative sites can be omitted during initial modeling of structure, or if there are many such ambiguous probes, then ribonuclease H digestion can be used to identify actual binding sites. After such filtering, the middle nucleotide of hybridized, single binding site probes can be used as equivalent to a site of chemical modification to deduce a model for the secondary structure using RNAstructure. To be acceptable, the structure generated also has to have at least one reasonable binding site for probes that bind but have multiple potential binding sites. If probes of different lengths are included on the microarray, then binding as a function of the length could be compared to the predicted structure as an additional test (*15*). A comparison of probe binding to loops found in the modeled structure may also provide insight into which loops are rigid and unusually stable as opposed to dynamic. For example, the lack of binding to loop E of *E. coli* 5S rRNA in the presence of Mg^{2+} indicates that loop E is rigid, which is consistent with its known properties (*22*, *23*, *63*, *66*). For *E. coli* 5S rRNA, this approach was able to provide a structure that contains 92% of known canonical base pairs, whereas free-energy minimization alone predicted only 27% of the known base pairs (Figure 4).

Interpretation of oligonucleotide-binding data will be facilitated in the future by the incorporation of modified nucleotides that equalize binding to unstructured RNA for all sequences, by improved understanding of the thermodynamics of binding, including the temperature dependence, and by the development of algorithms to take advantage of these advances. For example, programs such as OligoWalk (*50*) could be expanded to include contributions from coaxial stacking involving oligonucleotide and could be used to automatically compare binding observed to a microarray to that predicted for all possible secondary structures generated by other algorithms (*6*, *7*, *13*, *68*−*72*). New methods for detecting binding to microarrays eliminate the necessity for labeling the target (*73*) and provide the possibility of further automating the readout and interpretation of microarray results. The method should also provide insight into loops that provide good targets for antisense (*74*−*77*) and RNAi (*78*, *79*) approaches to therapeutics. For example, rigid loops such as loop E will not provide good targets for therapeutics composed of nucleic acids.

ACKNOWLEDGMENT

I. E. C. and D. H. T. thank Drs. M. D. Disney and J. L. Childs for help in initiating this project. We also thank Professor Peter B. Moore for the gift of *E. coli* plasmid pKK5-1.

SUPPORTING INFORMATION AVAILABLE

Table with results for all tested probes. This material is available free of charge via the Internet at http://pubs.acs.org.

REFERENCES

1. Fox, G. E., and Woese, C. R. (1975) 5S-RNA secondary structure, *Nature 256*, 505−507.
2. Pace, N. R., Thomas, B. C., and Woese, C. R. (1999) Probing RNA structure, function, and history by comparative analysis, in *The RNA World* (Gesteland, R. F., Cech, T. R., Atkins, J. F., Eds.) pp 113−141, Cold Spring Harbor Press, New York.
3. Goertzen, L. R., Cannone, J. J., Gutell, R. R., and Jansen, R. K. (2003) ITS secondary structure derived from comparative analysis: Implications for sequence alignment and phylogeny of the Asteraceae, *Mol. Phylogenet. Evol. 29*, 216−234.
4. Cannone, J. J., Subramanian, S., Schnare, M. N., Collett, J. R., D'Souza, L. M., Du, Y. S., Feng, B., Lin, N., Madabusi, L. V., Muller, K. M., Pande, N., Shang, Z. D., Yu, N., and Gutell, R. R. (2002) The Comparative RNA Web (CRW) Site: An online database of comparative sequence and structure information for ribosomal, intron, and other RNAs, *BMC Bioinf. 3*.
5. Macke, T. J., Ecker, D. J., Gutell, R. R., Gautheret, D., Case, D. A., and Sampath, R. (2001) RNAMotif, an RNA secondary structure definition and search algorithm, *Nucleic Acids Res. 29*, 4724−4735.
6. Zuker, M. (1989) On finding all suboptimal foldings of an RNA molecule, *Science 244*, 48−52.
7. Mathews, D. H., Sabina, J., Zuker, M., and Turner, D. H. (1999) Expanded sequence dependence of thermodynamic parameters improves prediction of RNA secondary structure, *J. Mol. Biol. 288*, 911−940.
8. Tinoco, I., Borer, P. N., Dengler, B., Levine, M. D., Uhlenbeck, O. C., Crothers, D. M., and Gralla, J. (1973) Improved estimation of secondary structure in ribonucleic acids, *Nature, New Biol. 246*, 40−41.
9. Xia, T. B., SantaLucia, J., Burkard, M. E., Kierzek, R., Schroeder, S. J., Jiao, X. Q., Cox, C., and Turner, D. H. (1998) Thermodynamic parameters for an expanded nearest-neighbor model for formation of RNA duplexes with Watson−Crick base pairs, *Biochemistry 37*, 14719−14735.
10. Xia, T. B., Mathews, D. H., and Turner, D. H. (1999) Thermodynamics of RNA secondary structure formation, in *Prebiotic Chemistry, Molecular Fossils, Nucleosides, and RNA* (Soll, D. G., Nishimura, S., and Moore, P. B., Eds.) pp 21−48, Elsevier, New York.
11. Turner, D. H. (2000) Conformational changes, in *Nucleic Acids* (Bloomfield, V. A., Crothers, D. M., and Tinoco, I., Eds.) pp 259−334, University Science Book, Sausalito, CA.
12. Zuker, M., and Stiegler, P. (1981) Optimal computer folding of large RNA sequences using thermodynamics and auxiliary information, *Nucleic Acids Res. 9*, 133−148.
13. Mathews, D. H., Disney, M. D., Childs, J. L., Schroeder, S. J., Zuker, M., and Turner, D. H. (2004) Incorporating chemical modification constraints into a dynamic programming algorithm for prediction of RNA secondary structure, *Proc. Natl. Acad. Sci. U.S.A. 101*, 7287−7292.
14. Uhlenbeck, O. C., Baller, J., and Doty, P. (1970) Complementary oligonucleotide binding to the anticodon loop of fMet transfer RNA, *Nature 225*, 508−510.
15. Uhlenbeck, O. C. (1972) Complementary oligonucleotide binding to transfer RNA, *J. Mol. Biol. 65*, 25−41.
16. Lewis, J. B., and Doty, P. (1970) Derivation of the secondary structure of 5S RNA from its binding of complementary oligonucleotides, *Nature 225*, 510−512.
17. Milner, N., Mir, K. U., and Southern, E. M. (1997) Selecting effective antisense reagents on combinatorial oligonucleotide arrays, *Nat. Biotechnol. 15*, 537−541.
18. Sohail, M., Akhtar, S., and Southern, E. M. (1999) The folding of large RNAs studied by hybridization to arrays of complementary oligonucleotides, *RNA 5*, 646−655.
19. Sohail, M., Hochegger, H., Klotzbucher, A., Le Guellec, R., Hunt, T., and Southern, E. M. (2001) Antisense oligonucleotides selected by hybridization to scanning arrays are effective reagents *in vivo*, *Nucleic Acids Res. 29*, 2041−2051.
20. Chechetkin, V. R., Turygin, A. Y., Proudnikov, D. Y., Prokopenko, D. V., Kirillov, E. V., and Mirzabekov, A. D. (2000) Sequencing by hybridization with the generic 6-mer oligonucleotide microarray: An advanced scheme for data processing, *J. Biomol. Struct. Dyn. 18*, 83−101.
21. Szymanski, M., Specht, T., Barciszewska, M. Z., Barciszewski, J., and Erdmann, V. A. (1998) 5S rRNA data bank, *Nucleic Acids Res. 26*, 156−159.
22. Dallas, A., and Moore, P. B. (1997) The loop E loop D region of *Escherichia coli* 5S rRNA: The solution structure reveals an unusual loop that may be important for binding ribosomal proteins, *Structure 5*, 1639−1653.
23. Correll, C. C., Freeborn, B., Moore, P. B., and Steitz, T. A. (1997) Metals, motifs, and recognition in the crystal structure of a 5S rRNA domain, *Cell 91*, 705−712.
24. Ban, N., Nissen, P., Hansen, J., Moore, P. B., and Steitz, T. A. (2000) The complete atomic structure of the large ribosomal subunit at 2.4 Å resolution, *Science 289*, 905−920.
25. Ciesiolka, J., Lorenz, S., and Erdmann, V. A. (1992) Different conformational forms of *Escherichia coli* and rat liver 5S ribosomal RNA revealed by Pb^{II}-induced hydrolysis, *Eur. J. Biochem. 204*, 583−589.
26. Goringer, H. U., and Wagner, R. (1988) 5S RNA structure and function, *Method Enzymol. 164*, 721−747.
27. Christensen, A., Mathiesen, M., Peattie, D., and Garrett, R. A. (1985) Alternative conformers of 5S ribosomal-RNA and their biological relevance, *Biochemistry 24*, 2284−2291.
28. Weidner, H., Yuan, R., and Crothers, D. M. (1977) Does 5S RNA function by a switch between two secondary structures? *Nature 266*, 193−194.
29. Caruthers, M. H., Beaton, G., Wu, J. V., and Wiesler, W. (1992) Chemical synthesis of deoxyoligonucleotides and deoxyoligonucleotide analogs, *Methods Enzymol. 211*, 3−20.
30. Matteucci, M. D., and Caruthers, M. H. (1980) Nucleotide chemistry. 1. Synthesis of oligodeoxypyrimidines on a polymer support, *Tetrahedron Lett. 21*, 719−722.
31. Puglisi, J. D., and Tinoco, I. (1989) Absorbency melting curves of RNA, *Methods Enzymol. 180*, 304−325.
32. Moore, P. B., Abo, S., Freeborn, B., Gewirth, D. T., Leontis, N. B., and Sun, G. (1988) Preparation of 5S RNA-related materials for nuclear magnetic resonance and crystallography studies, *Methods Enzymol. 164*, 158−174.
33. Merino, E. J., Wilkinson, K. A., Coughlan, J. L., and Weeks, K. M. (2005) RNA structure analysis at single nucleotide resolution by selective 2′-hydroxyl acylation and primer extension (SHAPE), *J. Am. Chem. Soc. 127*, 4223−4231.
34. Ziehler, W. A., and Engelke, D. R. (2000) Probing RNA structure with chemical reagents and enzymes, *Curr. Protoc. Nucleic Acid Chem. 2*, 6.1.1−6.1.21.
35. Wilkinson, K. A., Merino, E. J., and Weeks, K. M. (2005) RNA SHAPE chemistry reveals nonhierarchical interactions dominate equilibrium structural transitions in tRNA(Asp) transcripts, *J. Am. Chem. Soc. 127*, 4659−4667.
36. Afanassiev, V. H., V., and Wölfl, S. (2000) Preparation of DNA and protein micro arrays on glass slides coated with an agarose film, *Nucleic Acids Res. 28*, e66.
37. McDowell, J. A., and Turner, D. H. (1996) Investigation of the structural basis for thermodynamic stabilities of tandem GU mismatches: Solution structure of $(rGAGGUCUC)_2$ by two-dimensional NMR and simulated annealing, *Biochemistry 35*, 14077−14089.
38. Ehresmann, C., Baudin, F., Mougel, M., Romby, P., Ebel, J. P., and Ehresmann, B. (1987) Probing the structure of RNAs in solution, *Nucleic Acids Res. 15*, 9109−9128.
39. Moazed, D., Stern, S., and Noller, H. F. (1986) Rapid chemical probing of conformation in 16-S ribosomal-RNA and 30-S ribosomal-subunits using primer extension, *J. Mol. Biol. 187*, 399−416.
40. Douthwaite, S., and Garrett, R. A. (1981) Secondary structure of prokaryotic 5S ribosomal ribonucleic-acids−A study with ribonucleases, *Biochemistry 20*, 7301−7307.
41. Brunel, C., Romby, P., Westhof, E., Ehresmann, C., and Ehresmann, B. (1991) 3-Dimensional model of *Escherichia coli* ribosomal 5-S RNA as deduced from structure probing in solution and computer modeling, *J. Mol. Biol. 221*, 293−308.
42. Goringer, H. U., and Wagner, R. (1986) Does 5S RNA from *Escherichia coli* have a pseudoknotted structure? *Nucleic Acids Res. 14*, 7473−7485.
43. Manning, G. S. (1978) Molecular theory of polyelectrolyte solutions with applications to electrostatic properties of polynucleotides, *Q. Rev. Biophys. 11*, 179−246.
44. Demarky, N., and Manning, G. S. (1975) Application of polyelectrolyte limiting laws to helix−coil transition of DNA. 3. Dependence of helix stability on excess univalent salt and on polynucleotide phosphate concentration for variable equivalent ratios of divalent metal-ion to phosphate, *Biopolymers 14*, 1407−1422.

45. Crooke, S. T., Lemonidis, K. M., Neilson, L., Griffey, R., Lesnik, E. A., and Monia, B. P. (1995) Kinetic characteristics of *Escherichia coli* RNase H1−Cleavage of various antisense oligonucleotide−RNA duplexes, *Biochem. J. 312*, 599−608.
46. Monia, B. P., Lesnik, E. A., Gonzalez, C., Lima, W. F., McGee, D., Guinosso, C. J., Kawasaki, A. M., Cook, P. D., and Freier, S. M. (1993) Evaluation of 2′-modified oligonucleotides containing 2′-deoxy gaps as antisense inhibitors of gene expression, *J. Biol. Chem. 268*, 14514−14522.
47. Jin, R. Z., Gaffney, B. L., Wang, C., Jones, R. A., and Breslauer, K. J. (1992) Thermodynamics and structure of a DNA tetraplex−A spectroscopic and calorimetric study of the tetramolecular complexes of d(TG_3T) and d($TG_3T_2G_3T$), *Proc. Natl. Acad. Sci. U.S.A. 89*, 8832−8836.
48. Sen, D., and Gilbert, W. (1990) A sodium−potassium switch in the formation of 4-stranded G4-DNA, *Nature 344*, 410−414.
49. Sen, D., and Gilbert, W. (1988) Formation of parallel 4-stranded complexes by guanine-rich motifs in DNA and its implications for meiosis, *Nature 334*, 364−366.
50. Mathews, D. H., Burkard, M. E., Freier, S. M., Wyatt, J. R., and Turner, D. H. (1999) Predicting oligonucleotide affinity to nucleic acid targets, *RNA 5*, 1458−1469.
51. Kierzek, E., Ciesielska, A., Pasternak, K., Mathews, D. H., Turner, D. H., and Kierzek, R. (2005) The influence of locked nucleic acid residues on the thermodynamic properties of 2′-*O*-methyl RNA/RNA heteroduplexes, *Nucleic Acids Res. 33*, 5082−5093.
52. Walter, A. E., and Turner, D. H. (1994) Sequence dependence of stability for coaxial stacking of RNA helixes with Watson−Crick base paired interfaces, *Biochemistry 33*, 12715−12719.
53. He, L., Kierzek, R., SantaLucia, J., Walter, A. E., and Turner, D. H. (1991) Nearest-neighbor parameters for GU mismatches−5′GU3′/3′UG5′ is destabilizing in the contexts CGUG/GUGC, UGUA/AUGU, and AGUU/UUGU but stabilizing in GGUC/CUGG, *Biochemistry 30*, 11124−11132.
54. Agris, P. F., Sierzputowska-Gracz, H., Smith, W., Malkiewicz, A., Sochacka, E., and Nawrot, B. (1992) Thiolation of uridine carbon-2 restricts the motional dynamics of the transfer-RNA wobble position nucleoside, *J. Am. Chem. Soc. 114*, 2652−2656.
55. Smith, W. S., Sierzputowska-Gracz, H., Sochacka, E., Malkiewicz, A., and Agris, P. F. (1992) Chemistry and structure of modified uridine dinucleosides are determined by thiolation, *J. Am. Chem. Soc. 114*, 7989−7997.
56. Kumar, R. K., and Davis, D. R. (1997) Synthesis and studies on the effect of 2-thiouridine and 4-thiouridine on sugar conformation and RNA duplex stability, *Nucleic Acids Res. 25*, 1272−1280.
57. Testa, S. M., Disney, M. D., Turner, D. H., and Kierzek, R. (1999) Thermodynamics of RNA−RNA duplexes with 2- or 4-thiouridines: Implications for antisense design and targeting a group I intron, *Biochemistry 38*, 16655−16662.
58. Okamoto, I., Shohda, K., Seio, K., and Sekine, M. (2003) A new route to 2′-*O*-alkyl-2-thiouridine derivatives via 4-*O*-protection of the uracil base and hybridization properties of oligonucleotides incorporating these modified nucleoside derivatives, *J. Org. Chem. 68*, 9971−9982.
59. Knapp, G. (1989) Enzymatic approaches to probing of RNA secondary and tertiary structure, *Methods Enzymol. 180*, 192−212.
60. Mir, K. U., and Southern, E. M. (1999) Determining the influence of structure on hybridization using oligonucleotide arrays, *Nat. Biotechnol. 17*, 788−792.
61. Majlessi, M., Nelson, N. C., and Becker, M. M. (1998) Advantages of 2′-*O*-methyl oligoribonucleotide probes for detecting RNA targets, *Nucleic Acids Res. 26*, 2224−2229.
62. Sugimoto, N., Nakano, S., Katoh, M., Matsumura, A., Nakamuta, H., Ohmichi, T., Yoneyama, M., and Sasaki, M. (1995) Thermodynamic parameters to predict stability of RNA/DNA hybrid duplexes, *Biochemistry 34*, 11211−11216.
63. Serra, M. J., Baird, J. D., Dale, T., Fey, B. L., Retatagos, K., and Westhof, E. (2002) Effects of magnesium ions on the stabilization of RNA oligomers of defined structures, *RNA 8*, 307−323.
64. Gabashvili, I. S., Whirl-Carrillo, M., Bada, M., Banatao, D. R., and Altman, R. B. (2003) Ribosomal dynamics inferred from variations in experimental measurements, *RNA 9*, 1301−1307.
65. Pieler, T., Digweed, M., and Erdmann, V. A. (1985) RNA structural dynamics−Pre-melting and melting transitions in *Escherichia coli* 5S ribosomal RNA, *J. Biomol. Struct. Dyn. 3*, 495−514.
66. Leontis, N. B., and Westhof, E. (1998) The 5S rRNA loop E: Chemical probing and phylogenetic data versus crystal structure, *RNA 4*, 1134−1153.
67. Diamond, J. M., Turner, D. H., and Mathews, D. H. (2001) Thermodynamics of three-way multibranch loops in RNA, *Biochemistry 40*, 6971−6981.
68. Wuchty, S., Fontana, W., Hofacker, I. L., and Schuster, P. (1999) Complete suboptimal folding of RNA and the stability of secondary structures, *Biopolymers 49*, 145−165.
69. Gultyaev, A. P., Vanbatenburg, F. H. D., and Pleij, C. W. A. (1995) The computer-simulation of RNA folding pathways using a genetic algorithm, *J. Mol. Biol. 250*, 37−51.
70. Rivas, E., and Eddy, S. R. (1999) A dynamic programming algorithm for RNA structure prediction including pseudoknots, *J. Mol. Biol. 285*, 2053−2068.
71. Ding, Y., and Lawrence, C. E. (2003) A statistical sampling algorithm for RNA secondary structure prediction, *Nucleic Acids Res. 31*, 7280−7301.
72. Dirks, R. M., and Pierce, N. A. (2003) A partition function algorithm for nucleic acid secondary structure including pseudoknots, *J. Comput. Chem. 24*, 1664−1677.
73. Lu, J. H., Strohsahl, C. M., Miller, B. L., and Rothberg, L. J. (2004) Reflective interferometric detection of label-free oligonucleotides, *Anal. Chem. 76*, 4416−4420.
74. Stephenson, M. L., and Zamecnik, P. C. (1978) Inhibition of Rous-Sarcoma viral-RNA translation by a specific oligodeoxyribonucleotide, *Proc. Natl. Acad. Sci. U.S.A. 75*, 285−288.
75. Zamecnik, P. C., and Stephenson, M. L. (1978) Inhibition of Rous-Sarcoma virus-replication and cell transformation by a specific oligodeoxynucleotide, *Proc. Natl. Acad. Sci. U.S.A. 75*, 280−284.
76. Agrawal, S., Mayrand, S. H., Zamecnik, P. C., and Pederson, T. (1990) Site-specific excision from RNA by RNase-H and mixed-phosphate-backbone oligodeoxynucleotides. *Proc. Natl. Acad. Sci. U.S.A. 87*, 1401−1405.
77. Agrawal, S., Jiang, Z. W., Zhao, Q. Y., Shaw, D., Cai, Q. Y., Roskey, A., Channavajjala, L., Saxinger, C., and Zhang, R. W. (1997) Mixed-backbone oligonucleotides as second generation antisense oligonucleotides: *In vitro* and *in vivo* studies, *Proc. Natl. Acad. Sci. U.S.A. 94*, 2620−2625.
78. Schwarz, D. S., Hutvagner, G., Du, T., Xu, Z. S., Aronin, N., and Zamore, P. D. (2003) Asymmetry in the assembly of the RNAi enzyme complex, *Cell 115*, 199−208.
79. Khvorova, A., Reynolds, A., and Jayasena, S. D. (2003) Functional siRNAs and rniRNAs exhibit strand bias, *Cell 115*, 209−216.

BI051409+